Low Resolution Structural Models of the Basic Helix-Loop-Helix Leucine Zipper Domain of Upstream Stimulatory Factor 1 and Its Complexes with DNA from Small Angle X-Ray Scattering Data

Ekaterina P. Lamber,*[†] Matthias Wilmanns,* and Dmitri I. Svergun*[‡]
*European Molecular Biology Laboratory, Hamburg Outstation, D-22603 Hamburg, Germany; [†]Harvard Medical School and Brigham and Women's Hospital, Boston, Massachusetts 02115; and [‡]Institute of Crystallography, Russian Academy of Sciences, 117333 Moscow, Russia

ABSTRACT   The upstream stimulatory factor 1 (USF1) belongs to the basic helix-loop-helix leucine zipper (b/HLH/Z) transcription factor family, recognizing the CACGTG DNA motive as a dimer and playing an important role in the regulation of transcription in a variety of cellular and viral promoters. In this study we investigate the USF1 b/HLH/Z domain and its complexes with DNA by small angle x-ray scattering. We present low resolution structural models of monomeric b/HLH/Z USF1 in the absence of DNA and USF1 dimeric $(b/HLH/Z)_2$-DNA and tetrameric $(b/HLH/Z)_4$-DNA_2 complexes. The data reveal a concentration-dependent USF1 dimer $(b/HLH/Z)_2$-DNA-tetramer $(b/HLH/Z)_4$-DNA_2 equilibrium. The ability of b/HLH/Z USF1 to form a tetrameric assembly on two distant DNA binding sites as a consequence of increased protein concentration suggest a USF1 concentration-dependant mechanism of transcription activation involving DNA loop formation.

INTRODUCTION

The human upstream stimulatory factor 1 (USF1) is a basic helix-loop-helix leucine zipper (b/HLH/Z) transcription factor important for the activation of transcription on a variety of cellular and viral promoters (1,2). It binds as a dimer to the common CACGTG element, known as the E-box via its b/HLH/Z DNA binding domain (3). The leucine zipper fragment has been shown to be important for high DNA affinity (3).

Two or more USF1 binding sites were found on several cellular and viral promoters, whereby one USF1 binding site was located upstream to the promoter and the second and sometimes the third site were located downstream to the promoter (1,2). One example of a promoter with two USF1 binding sites is the human telomerase reverse transcriptase promoter (1). Mutations of each of the USF1 binding sites decrease the promoter response to USF1 (1). When binding to the human immunodeficiency virus (HIV1) long terminal repeat, besides the E-box in the distal enhancer USF1 interacts with two initiator elements located near the transcription start site (2). Moreover, the adenovirus major late promoter comprises one USF1 binding site in the distal part of the promoter and two sites in the initiator element. Mutations in each of the three USF1 binding sites decrease the adenovirus major late and HIV1 promoter activity (2).

Previous spectroscopic and biochemical experiments demonstrated that the b/HLH/Z domain of USF1 can form bivalent homotetramers when bound to two recognition sequences (3,4). It was suggested that the homotetramer formation may lead to the DNA looping, which may allow the recruitment of USF1 and other factors from the distal region of the promoter to the initiator element (3). A model of anticooperative DNA binding was suggested based on stop flow kinetics data (4).

Several studies have focused on USF1 transcription factor function and described USF1 homotetramerization on two independent DNA binding sites, resulting in the DNA loop formation (3). Nevertheless, there is no structural information on the b/HLH/Z domain of USF1 in the absence of DNA, USF1 dimeric $(b/HLH/Z)_2$-DNA, and tetrameric $(b/HLH/Z)_4$-DNA_2 complexes.

In this work we employ small angle x-ray scattering (SAXS) to structurally characterize free b/HLH/Z domain of USF1 and to investigate the oligomerization properties and low resolution structures of b/HLH/Z USF1 complexes with DNA. The low resolution models from solution scattering data have been obtained independently using ab initio methods and also by rigid body modeling. We demonstrate that free b/HLH/Z USF1 is a monomer in the solution and reveals an elongated shape. Moreover, we present low resolution models of USF1 dimeric $(b/HLH/Z)_2$-DNA and tetrameric $(b/HLH/Z)_4$-DNA_2 complexes, demonstrating a concentration-dependant dimer-tetramer equilibrium.

MATERIALS AND METHODS

b/HLH/Z USF1 expression and purification

The complementary DNA (cDNA) sequence coding for b/HLH/Z USF1 residues 197–310 was amplified by polymerase chain reaction and cloned into the expression vector pProExHTb carrying an N-terminal His-tag sequence and a tobacco etch virus protease cleavage site. The two cysteins of this construct (residues 229 and 248) were mutated into serines by site-directed mutagenesis. The protein fragment was overexpressed in *Escherichia coli* strain BL21(DE3)CodonPlus-RIL induced with 1 mM IPTG (isopropyl β-D-thiogalactopyranoside) at 37°C for 1.5 h. Cell pellets were resuspended in a lysis buffer (20 mM Tris-HCl pH 8.0, 300 mM NaCl, 5 mM

imidazole) containing additionally EDTA-free protease inhibitor mix (Roche, Basel, Switzerland), lysozyme and DNase I and sonicated. b/HLH/Z USF1 was purified from the soluble cellular fraction by nickel-nitrilotriacetic acid affinity chromatography. The hexahistidine-tag was removed by adding TEV-protease. The cleaved protein was further purified using an ion exchange chromatography (Amersham, Buckinghamshire, UK; Mono S column). The final purification step was done by size exclusion chromatography, using a Superdex 75 16/60 (Amersham) preequilibrated with 20 mM Tris-HCl pH 8.0 containing 100 mM NaCl and 2 mM EDTA.

b/HLH/Z USF1/DNA complex formation and purification by gel filtration

b/HLH/Z USF1 complexes with DNA were formed by mixing the protein obtained after gel filtration purification and DNA at a molar ratio of 2:1 (protein/DNA). A 15 bp double-stranded DNA (dsDNA) fragment containing USF1 binding site (E-box) was used (Fig. 1). The complex was purified by size exclusion chromatography, using a Superdex 75 16/60 (Amersham) preequilibrated with 20 mM Tris-HCl pH 8.0 containing 100 mM NaCl and 2 mM EDTA.

SAXS data collection and analysis

Synchrotron SAXS data were collected on the EMBL X33 camera with a linear gas detector (5) on the storage ring DORIS III (Deutsches Elektronen-Synchrotron (DESY), Hamburg, Germany). All samples were measured for at least three solute concentrations ranging from 1 mg/ml to 8 mg/ml. The data were processed by the program PRIMUS (6) following standard procedures (7) to compute the radii of gyration (R_g) and maximum dimensions (D_{max}). The distance distribution functions, $p(r)$, were evaluated using the program GNOM (8). The molecular masses of the solutes were estimated by calibration against reference solutions of bovine serum albumin. The excluded particle volumes V_p were computed from the scattering data using Porod invariant (9).

Low resolution models of b/HLH/Z USF1 were generated by the ab initio program GASBOR (10), which represents a protein by an assembly of a fixed number, M, dummy residues (DRs). Starting from a random gas of residues, simulated annealing is employed to build a locally ''chain-compatible'' DR model inside a spherical search volume with diameter D_{max} to minimize discrepancy with the experimental pattern $I(s)$:

$$\chi^2 = \frac{1}{N-1} \sum_j \left[\frac{I(s_j) - c I_{calc}(s_j)}{\sigma(s_j)} \right]^2, \quad (1)$$

where N is the number of experimental points, c is a scaling factor, and $I_{calc}(s)$ and $\sigma(s_j)$ are the calculated intensity and the experimental error at the momentum transfer s_j, respectively. The only restraint to the GASBOR model was the total number of the b/HLH/Z USF1 residues ($M = 120$) taken from the protein sequence.

The results of 10 independent GASBOR runs were averaged by the package DAMAVER (11). The individual models were superimposed using the program SUPCOMB (12) and analyzed to select the most typical model (i.e., the model displaying the lowest deviation from the rest models) and to construct the average model representing common structural features of all the reconstructions.

5' − tcat*CACGTG*gcccg
3' − agta*GTGCAC*cgggc

FIGURE 1 A 15 bp dsDNA fragment containing USF1 binding site (E-box). The core binding sequence is a palindrome of six bases (shown in italic).

Molecular modeling

The models of the USF1 dimeric (b/HLH/Z)$_2$-DNA and tetrameric (b/HLH/Z)$_4$-DNA$_2$ complexes were created interactively from the high resolution structures of USF1 (b/HLH)$_2$-DNA (without leucine zipper) (3) and of the leucine zipper fragment taken from a Max (b/HLH/Z)$_2$-DNA complex (13) by using the program MASSHA (14). The scattering patterns of the atomic models were calculated by the program CRYSOL (15). The volume fractions of USF1 (b/HLH/Z)$_2$-DNA and (b/HLH/Z)$_4$-DNA$_2$ complexes in the mixtures were computed by the program OLIGOMER (6), minimizing discrepancy in Eq. 1 between the linear combination of the intensities of the two components and the experimental data from the mixture.

RESULTS

b/HLH/Z USF1 /DNA complex formation and purification

The formation of a stable b/HLH/Z USF1/DNA complex is evidenced by electrophoresis, suggesting an equilibrium of dimers and tetramers (Fig. 2), and its oligomerization state was further analyzed by gel filtration. The complex came out of the gel filtration column as a single peak, and its molecular weight was measured by static light scattering to be a dimer of b/HLH/Z USF1 bound to DNA. However, the sample concentration after gel filtration was ~0.3–0.5 mg/ml (which
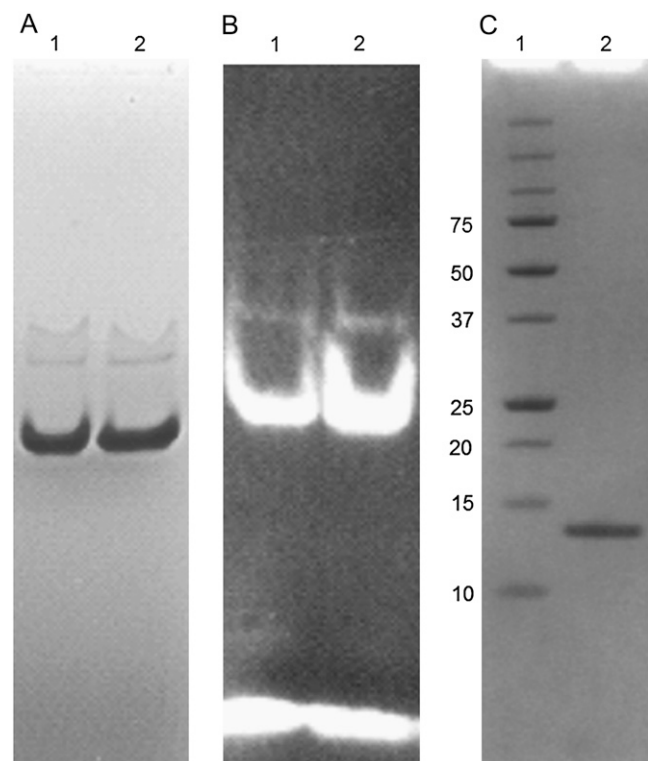

FIGURE 2 Native gel and sodium dodecyl sulfate-polyacrylamide gel electrophoresis (SDS-PAGE) of b/HLH/Z USF1/DNA complexes. (*A* and *B*) Gels stained with Coomassie blue and ethidium bromide, respectively. Lanes 1, 2: USF1/DNA complex, upper bands correspond to homotetramer, lower bands to dimer. On the ethidium bromide stained gel the bottom band corresponds to free DNA. (*C*) SDS-PAGE of the USF1/DNA complex. Lane 1: molecular weight marker, lane 2: USF1.

would correspond to 3.5–5.8 μM). For the more concentrated samples both tetramers and dimers were observed on the native gel (Fig. 2), indicating that b/HLH/Z USF1/DNA complexes may have a concentration-dependent dimer-tetramer equilibrium in solution.

SAXS analysis of b/HLH/Z USF1/DNA complexes

The scattering patterns from the b/HLH/Z USF1/DNA complexes at different solute concentrations are presented in Fig. 3 (*curves* 1 and 2). The overall parameters of the solute in Table 1 (radius of gyration R_g, excluded particle volume V_p, and maximum dimension D_{max}) clearly increase with the solute concentration. The absolute V_p values in Table 1 are somewhat lower than those expected from the chemical composition (e.g., for a dimeric complex the excluded volume is 30 nm^3 for the protein part and 8.6 nm^3 for the DNA part, assuming the partial specific volumes of the two components, 0.74 g/cm^3 and 0.56 g/cm^3, respectively). This can be explained by limited accuracy of Porod approximation (9) assuming particle uniformity for a protein/DNA complex. Still, the fact that the twofold concentration increase doubles the excluded volume clearly indicates different oligomerization states at lower and higher complex concentrations. Similarly, although due to the presence of DNA the molecular mass of the complex could not be accurately determined by normalization against the bovine serum albumin solution,
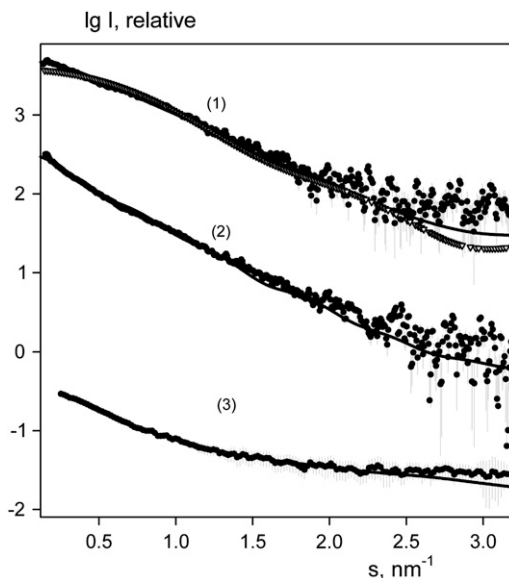

FIGURE 3 Experimental and calculated scattering patterns of b/HLH/Z USF1 dimer bound to DNA (*1*), b/HLH/Z USF1 tetramer bound to DNA (*2*), and free b/HLH/Z USF1 (*3*). The experimental SAXS data are displaced as dots with error bars, the patterns computed from the as solid curves. For the USF1 dimer (solute concentration 2 mg/ml), triangles and solid curve represent the fits from the models b/HLH without leucine zipper fragment (*3*), and with this fragment added, respectively. For b/HLH/Z UFS1 tetramer (solute concentration 6 mg/ml), the fit from the best rigid body model (displayed in Fig. 4 *B*) is shown. For free b/HLH/Z USF1, the fit from the ab initio model in Fig. 4 *D* is presented.

a roughly twofold increase in the effective molecular mass was also observed with growing concentration on a relative scale. Overall, at $c \leq 3$ mg/ml, the overall parameters suggest a dimeric complex; for $c \approx 6$ mg/ml tetramers are observed, whereas the intermediate concentration data point to a mixture of the two oligomers. This concentration-dependent equilibrium further confirms the results observed on the native gel.

First, the dimeric structure was modeled against the low concentration data. The scattering pattern computed from the USF1 (b/HLH)$_2$-DNA lacking leucine zipper fragment (3) displays systematic deviations from the experimental data with discrepancy $\chi = 1.4$, which was not surprising as the leucine zipper part was missing (Fig. 3, *curve* 1, *triangles*). To construct the model of the dimeric complex, the leucine zipper was taken from the crystal structure of the complex of the homologous protein b/HLH/Z Max with DNA (13) and interactively attached to the dimeric b/HLH USF1/DNA model (3) to best fit the experimental data. This model displayed in Fig. 4 *A* yielded a much better fit with $\chi = 1.2$ (Fig. 3, *curve* 1, *solid line*), and its structural parameters agreed well with the experimental values (Table 1).

Based on the USF1 (b/HLH/Z)$_2$-DNA model, a set of different models for the USF1 bivalent homotetramer bound to DNA, (b/HLH/Z)$_4$-DNA$_2$ was systematically screened against the scattering curve recorded at the complex concentration of 6 mg/ml. The best tentative model of the USF1 (b/HLH/Z)$_4$-DNA$_2$ providing the fit with $\chi = 1.7$ is shown in Fig. 3 (*curve* 2). Interestingly, this model displays the arrangement of the dimers very similar to that observed in the crystal structure of the homologous b/HLH/Z Myc-Max heterotetramer bound to DNA (16) as illustrated by the overlay in Fig. 4, *B* and *C*.

The models of the dimer and tetramer were further employed to analyze the scattering patterns at intermediate concentrations. The scattering curves recorded at concentrations in the range 3–4 mg/ml were fitted by the linear combinations of dimeric and tetrameric curves (Table 1), demonstrating an increase in the volume fraction of the tetramer with concentration. It may be concluded that the b/HLH/Z USF1/DNA complex forms tetramers similar to those of b/HLH/Z Myc-Max heterotetramer/DNA complex and dissociates into dimers at low solute concentrations ($c \leq 3$ mg/ml).

SAXS analysis of free b/HLH/Z USF1

The scattering pattern from the free b/HLH/Z USF1 in Fig. 3 (*curve* 3) yields the effective molecular mass of the solute of 11 ± 1 kDa, compatible with the value expected for the monomeric protein (13.7 kDa). The values of R_g and D_{max} (2.9 ± 0.2 nm and 11 ± 1 nm, respectively) indicate that the protein is very elongated in solution. Its low resolution structure reconstituted ab initio using the program GASBOR (10) fits the experimental data with $\chi = 0.9$ (Fig. 3, *curve* 3). The average ab initio model is superimposed in Fig. 4 *D* with

TABLE 1   Overall parameters of the b/HLH/Z USF1/DNA complexes

Sample concentration	R_g (nm)	D_{max} (nm)	V_p (nm^3)	Volume fractions (dimers/tetramers in percent)	Discrepancy χ^*
2 mg/ml	2.9 ± 0.1	10 ± 1	30 ± 2	100/0	1.2
3 mg/ml	3.3 ± 0.1	11 ± 1	32 ± 2	93 ± 3/7 ± 2	1.4
4 mg/ml	3.4 ± 0.1	12 ± 1	34 ± 5	73 ± 3/27 ± 3	1.9
6 mg/ml	4.0 ± 0.2	13 ± 1	63 ± 6	0/100	1.7
Models					
Dimer without zipper	1.9	7	27	—	—
Dimer with zipper	2.8	11	37	—	—
Tetramer	4.4	15	74	—	—

*For 2 and 6 mg/ml, fits by CRYSOL from dimer and tetramer model are given, respectively; for the intermediate concentrations, fits from best mixtures computed by OLIGOMER are presented. Structural parameters of the models were computed by CRYSOL (15).

the high resolution model of monomeric b/HLH/Z USF1 extracted from the model of the b/HLH/Z USF1 dimer bound to DNA. The comparison indicates that the b/HLH/Z USF1 monomer retains the overall shape as in the dimeric b/HLH/Z USF1 bound to DNA. On the other hand, the fit computed from the crystal structure is somewhat worse than that from the ab initio model ($\chi = 1.3$, fit not shown), and the R_g of the crystallographic monomer (2.7 nm) is lower than the experimental value. This may point to some flexibility of monomeric b/HLH/Z USF1 in solution discussed below.

DISCUSSION

We have used SAXS to analyze the low resolution structures of free b/HLH/Z USF1 in solution and of the complexes formed between b/HLH/Z USF1 and DNA. Free b/HLH/Z USF1 was an elongated molecule, monomeric in solution indicating that DNA is required to form dimers or tetramers. The free b/HLH/Z USF1 solutions were measured at solute concentrations below 2 mg/ml, as the protein had a tendency to aggregate at higher concentrations; however, no indications of specific dimerization were observed.

The ab initio model of b/HLH/Z USF1 reveals an overall low resolution shape similar to that of the b/HLH/Z USF1 monomer extracted from the SAXS model of b/HLH/Z USF1 dimer bound to the DNA. The overlap in Fig. 4 *D* also displays some deviations between the two models, which may indicate that b/HLH/Z USF1 is partially disordered in solution. This observation would agree with a circular dichroism spectroscopic study (3) where it was proposed that the DNA binding domain of USF1 is disordered and becomes folded by the interaction with specific DNA. The resolution of the ab initio SAXS model is not sufficient to provide a clear-cut answer; however the observed increase of the experimental R_g compared to that of the crystallographic monomer does support this hypothesis. This is the first time to our knowledge that a low resolution structural model has been provided for the b/HLH/Z USF1 in the absence of DNA.

The b/HLH/Z USF1/DNA complex displayed dimer/ tetramer equilibrium both in native gel and by SAXS. Using the latter method, the dimers and the tetramers could be characterized structurally, and their concentration-dependent

equilibrium was described in terms of the volume fractions of the two species. Moreover, the obtained tetrameric assemblies were compatible with those observed in the crystal structure of homologous b/HLH/Z Myc-Max transcription factor complex with DNA, although the latter was not use in the SAXS-based modeling. The analysis of the (b/HLH/Z USF1)$_4$-DNA$_2$ complex reveals that the homotetramerization involves leucine zipper as well as helix-loop fragment (residues 227–260). Moreover, our data indicate that the tetramerization of b/HLH/Z USF1 in the presence of DNA is concentration dependent. Taken together, our work provides low resolution structural models of (b/HLH/Z USF1)$_2$-DNA and (b/HLH/Z USF1)$_4$-DNA$_2$ and for the first time to our knowledge demonstrates a concentration-dependent USF1 tetramerization in the presence of DNA among the b/HLH/Z transcription factor family. Previous studies showed that b/HLH/Z USF1 binds DNA in a way that is undistinguishable from the full length protein (3). The results obtained here for the b/HLH/Z fragment, which is the DNA binding domain of USF1, should therefore hold for the full length protein as well.

Multiple USF1 binding sites (E-boxes) were observed for several viral and cellular promoters transcribed by RNA polymerase II. For HIV1 and adenovirus major late promoters, the USF1 binding sites are located on the distal region and the other USF1 binding sites are located on the initiator part of the promoter. The formation of the DNA loop was proposed previously (3) and the model of anticooperative USF1 binding to two distant USF1 binding sites was suggested based on the stop flow kinetics data (4). Our model of b/HLH/Z USF1 homotetramer bound to DNA lends support for the DNA looping theory due to the observed USF1 concentration-dependent tetramerization in the presence of DNA. Low USF1 concentration would lead to the USF1 dimer/DNA complex formation failing to form the DNA loop and therefore to a decrease in the promoter activity. In contrast, higher USF1 concentrations would lead to the USF1 tetramerization and DNA loop formation; as a result, transcription factors bound to the distal part of the promoter could interact with the initiator-bound transcription factors and stimulate transcription. Taken together, USF1 concentration dependant tetramerization might contribute to the
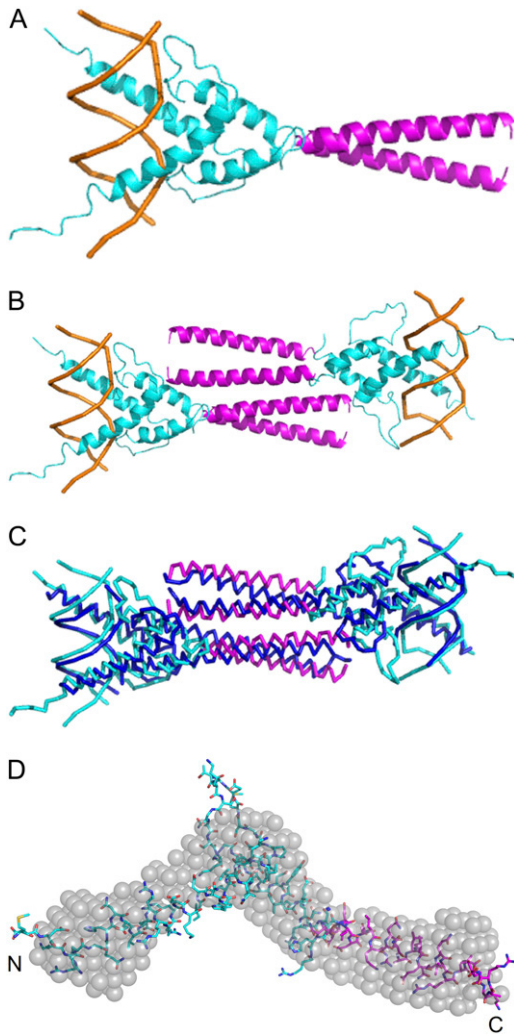
FIGURE 4 Comparison of the b/HLH/Z USF1 and b/HLH/Z USF1/DNA models from SAXS data and the crystallographic structures of the corresponding b/HLH/Z Myc-Max constructs. (*A*) The model of b/HLH/Z USF1 dimer/DNA obtained from SAXS data: b/HLH USF1 without leucine zipper fragment (3) is colored in cyan, the leucine zipper fragment extracted from crystallographic structure of b/HLH/Z Max/DNA complex (13) is colored in magenta, and the DNA is colored in orange. (*B*) The model of b/HLH/Z USF1 tetramer bound to DNA obtained by rigid body modeling against the SAXS data. (*C*) Comparison of the rigid body model of b/HLH/Z USF1 tetramer bound to DNA from SAXS and the b/HLH/Z Myc-Mac crystallographic tetramer. b/HLH USF1/DNA complex without leucine zipper fragment (3) is colored in cyan, the leucine zipper fragment extracted from crystallographic structure of Max/DNA complex (13) is colored in magenta. b/HLH/Z Myc-Mac tetramer in the complex with DNA (16) is colored in blue. (*D*) Comparison of the averaged ab initio b/HLH/Z USF1 model (*gray semitransparent beads*) with the crystallographic b/HLH/Z USF1 monomer (*cyan and magenta trace* with the same color code as in panel *A*).

DNA loop formation and therefore provide a novel mechanism of the transcription regulation. The employed methodology for the characterization of a protein/DNA complex with a tendency to oligomerize with increasing concentration

in terms of low resolution structural models and equilibrium mixtures demonstrates the potential of SAXS for the quantitative analysis of heterogeneous biological constructs showing dynamic equilibrium behavior in solution.

REFERENCES

1. Goueli, B. S., and R. Janknecht. 2003. Regulation of telomerase reverse transcriptase gene activity by upstream stimulatory factor. *Oncogene.* 22:8042–8047.

2. Du, H., A. L. Roy, and R. G. Roeder. 1993. Human transcription factor USF stimulates transcription through the initiator elements of the HIV-1 and the Ad-ML promoters. *EMBO J.* 12:501–511.

3. Ferre-D'Amare, A. R., P. Pognonec, R. G. Roeder, and S. K. Burley. 1994. Structure and function of the b/HLH/Z domain of USF. *EMBO J.* 13:180–189.

4. Sha, M., A. R. Ferre-D'Amare, S. K. Burley, and D. J. Goss. 1995. Anti-cooperative biphasic equilibrium binding of transcription factor upstream stimulatory factor to its cognate DNA monitored by protein fluorescence changes. *J. Biol. Chem.* 270:19325–19329.

5. Koch, M. H. J., and J. Bordas. 1983. X-ray diffraction and scattering on disordered systems using synchrotron radiation. *Nucl. Instrum. Methods.* 208:461–469.

6. Konarev, P. V., V. V. Volkov, A. V. Sokolova, M. H. J. Koch, and D. I. Svergun. 2003. PRIMUS—a Windows-PC based system for small-angle scattering data analysis. *J. Appl. Cryst.* 36:1277–1282.

7. Svergun, D. I., and M. H. J. Koch. 2003. Small angle scattering studies of biological macromolecules in solution. *Rep. Prog. Phys.* 66:1735–1782.

8. Svergun, D. I. 1992. Determination of the regularization parameter in indirect-transform methods using perceptual criteria. *J. Appl. Cryst.* 25:495–503.

9. Porod, G. 1982. General theory. *In* Small-Angle X-Ray Scattering. O. Glatter and O. Kratky, editors. Academic Press, London. 17–51.

10. Svergun, D. I., M. V. Petoukhov, and M. H. J. Koch. 2001. Determination of domain structure of proteins from x-ray solution scattering. *Biophys. J.* 80:2946–2953.

11. Konarev, P. V., M. V. Petoukhov, V. V. Volkov, and D. I. Svergun. 2006. ATSAS 2.1, a program package for small-angle scattering data analysis. *J. Appl. Cryst.* 39:277–286.

12. Kozin, M. B., and D. I. Svergun. 2001. Automated matching of high- and low-resolution structural models. *J. Appl. Cryst.* 34:33–41.

13. Ferre-D'Amare, A. R., G. C. Prendergast, E. B. Ziff, and S. K. Burley. 1993. Recognition by Max of its cognate DNA through a dimeric b/HLH/Z domain. *Nature.* 363:38–45.

14. Konarev, P. V., M. V. Petoukhov, and D. I. Svergun. 2001. MASSHA—a graphic system for rigid body modelling of macromolecular complexes against solution scattering data. *J. Appl. Cryst.* 34:527–532.

15. Svergun, D. I., C. Barberato, and M. H. J. Koch. 1995. CRYSOL—a program to evaluate x-ray solution scattering of biological macromolecules from atomic coordinates. *J. Appl. Cryst.* 28:768–773.

16. Nair, S. K., and S. K. Burley. 2003. X-ray structures of Myc-Max and Mad-Max recognizing DNA. Molecular bases of regulation by proto-oncogenic transcription factors. *Cell.* 112:193–205.